Molecular Cancer

RESEARCH

Open Access

Targeting m7G-enriched circKDM1A prevents colorectal cancer progression

Zhenqiang Sun[1,2,3*†], Yanxin Xu[1,2,3†], Chaohua Si[4,5†], Xiaoke Wu[6], Yaxin Guo[7], Chen Chen[2,3,4,7*] and Chengzeng Wang[2,3,8*]

Abstract

Plenty of circRNAs have been reported to play an important role in colorectal cancer (CRC), while the reason of abnormal circRNA expression in cancer still keep elusive. Here, we found that m7G RNA modifications were enriched in some circRNAs, these m7G modifications in circRNAs were catalyzed by METTL1, and the GG motif was the main site preference for m7G modifications in circRNAs. We further confirmed that METTL1 played a cancer-promoting role in CRC. We then screened a highly expressed circRNA, called circKDM1A, and found that METTL1 prevented the degradation of circKDM1A by m7G modification. CircKDM1A was further verified to promote proliferation, invasion and migration of CRC in vivo and in vitro. Its cancer-promoting ability was weakened after the m7G site mutation. CircKDM1A was verified to activate AKT pathway by upregulating PDK1, consequently promoting CRC progression. These results suggest that m7G-modified circRNA promotes CRC progression via activating AKT pathway. Our study uncovers an essential physiological function and mechanism of METTL1-mediated m7G modification in the regulation of circRNA stability and cancer progression.

Keywords M7G modification, circRNA, AKT pathway, Colorectal cancer (CRC)

†Zhenqiang Sun, Yanxin Xu and Chaohua Si contributed equally to this work.

*Correspondence:
Zhenqiang Sun
fccsunzq@zzu.edu.cn
Chen Chen
zzu2014cc@163.com
Chengzeng Wang
czw202112@zzu.edu.cn
[1]Department of Colorectal Surgery, The First Affiliated Hospital of Zhengzhou University, Zhengzhou 450052, Henan, China
[2]Henan Institute of Interconnected Intelligent Health Management, The First Affiliated Hospital of Zhengzhou University, Zhengzhou 450052, Henan, China
[3]Henan Key Laboratory of Chronic Disease Prevention and Therapy & Intelligent Health Management, The First Affiliated Hospital of Zhengzhou University, Zhengzhou 450052, Henan, China
[4]School of Life Science, Zhengzhou University, Zhengzhou 450001, Henan, China
[5]Academy of Medical Sciences, Zhengzhou University, Zhengzhou 450052, Henan, China
[6]Department of Neurology, The First Affiliated Hospital of Zhengzhou University, Zhengzhou 450052, Henan, China
[7]Department of Clinical Laboratory, The First Affiliated Hospital of Zhengzhou University, Zhengzhou 450052, Henan, China
[8]Department of Ultrasound, The First Affiliated Hospital of Zhengzhou University, Zhengzhou 450052, Henan, China

Introduction

Colorectal cancer (CRC) is the most common clinical malignant tumor of the digestive system, ranking fourth among cancers in incidence and second in mortality worldwide [1]. The occurrence and development of cancer is a complex process, and many problems remain to be solved. Therefore, we also need to explore more deeper molecular mechanisms of CRC development.

More than 100 different types of post-synthetic modifications have been shown to exist on RNA, including m6A, m5C, m7G [2]. It is currently reported that RNA modification affects the stability of mRNA and tRNA and affects RNA metabolism. For example, when m6A-containing mRNA is recognized by YTHDF2, the mRNA is rapidly degraded through the deadenylation pathway or the endoribonucleolytic pathway [3, 4]. When m6A is present at the 5' end of mRNA, it blocks its access to DCP2, thereby stabilizing the mRNA [5]. m7G interacts with C13-G22 in the D-loop to stabilize the tRNA tertiary structure, and the lack of m7G is associated with rapid tRNA decay and expression changes [6]. m6A modification is the most prevalent RNA modification in various types of RNA, including circRNA. The main functions of m6A modification of circRNAs in tumors include: (1) mediating the biogenesis of circRNA [7–9]; (2) maintaining the stability of circRNA [10, 11]; (3) promoting the cytoplasmic localization of circRNA [12].

m7G is one of the most prevalent modifications occurring in tRNA variable loops and is regulated by the human METTL1-WDR4 complex. As the "writer" of m7G, METTL1 is significantly overexpressed in AML, intrahepatic cholangiocarcinoma, hepatocellular carcinoma, bladder cancer, lung cancer and nasopharyngeal cancer and promotes tumor development, including affecting methylation levels of tRNA and tumor-related genes stability, cancer cell signaling pathways and other regulatory mechanisms [13–17]. Circular RNA (circRNA) is described as a type of end-to-end, single-stranded closed circular RNA molecule with high stability, conservation, and tissue expression specificity. Studies have shown that a variety of circRNAs can regulate tumor development, and the most studied ones are the regulation of tumor cells. Although both m7G modification and circRNA play an important role in promoting cancer, whether circRNA contains m7G modification and the other correlations between the two are still unclear, which requires further study. Here, we focused on the role of m7G-modified circRNA to explore its effect in CRC progression and the potential regulatory mechanism, which proved a new sight for targeted therapy for CRC.

Highlights

- A large number of m7G modifications were enriched on circRNA.
- Oncogenic METTL1 enhances circKDM1A stability via GG motif-dependent m7G modification.
- M7G modification increases the oncogenicity of circKDM1A in CRC.
- M7G-modified circKDM1A activates the AKT pathway via upregulating PDK1.

Methods

Patient tissue specimens and cell lines

Tissue from CRC patients were obtained from the First Affiliated Hospital of Zhengzhou University. A CRC tissue cDNA chip was obtained from Shanghai Outdo Biotech (Shanghai, China). All patients signed informed consent forms, and the protocols were approved by the Ethics Committee of the First Affiliated Hospital of Zhengzhou University (2019-KY-423) and Shanghai Outdo Biotech (YB M-05-02). HCT116 cells were obtained from the Shanghai Cell Bank of Chinese Academy of Sciences (Shanghai, China). SW480 cells and Human embryonic kidney 293T cells (293T cells) were generous gifts from the Biotherapy Center of the First Affiliated Hospital of Zhengzhou University. HCT116 cells and SW480 cells were cultured in high-glucose DMEM (Gibco, Carlsbad, CA, USA), 293T cells were cultured in RPMI 1640 (Gibco, Carlsbad, CA, USA) supplemented with 10% fetal bovine serum (Clark Bioscience, Richmond, VA, USA) at 37 ℃ and 5% CO_2.

M7G-RIP sequencing

The m7G-IP-Seq service was provided by CloudSeq Inc. (Shanghai, China). Total RNA from HCT116 cells was collected and processed using RNase R digestion. RNase R, an exonuclease, recognizes and binds to the 3' end of RNA molecules to degrade linear RNA and enrich circRNA, which lacks free 3' or 5' ends due to its closed loop structure. mRNA was then further isolated using oligo(dT) magnetic beads (ThermoFisher). Immunoprecipitation was performed according to the instructions of GenSeqTM m7G-IP kit (GenSeq Inc., China). RNA libraries for IP and input samples were then constructed with NEBNext® Ultra II Directional RNA Library Prep Kit (New England Biolabs, Inc., USA) by following the manufacturer's instructions. Libraries were qualified using Agilent 2100 bioanalyzer and then sequenced in a NovaSeq platform (Illumina). Briefly, Paired-end reads were harvested from Illumina NovaSeq 6000 sequencer, and were quality controlled by Q30. After 3'adaptor-trimming and low-quality reads removing by cutadapt software (v1.9.3). First, clean reads of input libraries were

aligned to reference genome (UCSC HG38) by STAR software. Then circRNAs were identified by DCC software using the STAR alignment results. After that, clean reads of all libraries were aligned to the reference genome by Hisat2 software (v2.0.4). Methylated sites on RNAs (peaks) were identified by MACS software. Differentially methylated sites were identified by diffReps. These peaks identified by both softwares overlapping with exons of mRNA, LncRNA and circRNA were figured out and chosen by home-made scripts. GO and Pathway enrichment analysis were performed by the differentially methylated protein coding genes, the associated genes of differentially methylated LncRNAs and the source genes of differentially methylated circRNAs separately.

SiMETTL1 sequencing

The SiMETTL1-seq service was provided by CloudSeq (Shanghai, China). SiRNAs targeting the backsplice junction site of METTL1 were synthesized by RiboBio (RiboBio, Guangzhou, China). Total RNA from HCT116 transfected si-METTL1 was purified using QIAGEN RNeasy Kit. Amplification was performed using the AffinityScript-RT kit using Cy3 labeling. After elution, raw images were obtained by scanning with an Agilent Scanner G5761A (Agilent Technologies). Feature Extraction software (version12.0.3.1, Agilent Technologies) was used to process the original image to extract the original data. Quantile normalization and subsequent processing were performed with the use of Genespring software (version14.8, Agilent Technologies). The normalized data were filtered so that at least one set of probes 100% labeled as detected from each set of samples used for comparison was left for subsequent analysis. The *p* value of T test was used to screen differentially expressed genes. Then, GO and KEGG enrichment analysis were performed to determine the main biological functions or pathways affected by the differential genes. Finally, unsupervised hierarchical clustering was performed on the differentially expressed genes, and the expression patterns of differentially expressed genes among different samples were displayed in the form of heat maps.

SiRNA and plasmid construction

The full-length of circKDM1A was cloned into over expression vector pcDNA3.1 (Hanbio Biotechnology, Wuhan, China), while the mock vector with no circKDM1A sequence served as a control. SiRNAs targeting the backsplice junction site of circKDM1A and METTL1 were synthesized by RiboBio (RiboBio, Guangzhou, China). Moreover, the shMETTL1 were synthesized by GenePharma (GenePharma, Shanghai, China), efficiency detected by qRT-PCR. miR-147b-3p mimics were purchased from RiboBio (RiboBio, Guangzhou, China). The wild-type and mutant circKDM1A plasmids were synthesized by Genechem (Genechem, Shanghai, China). The wild-type and mutant METTL1 were synthesized by Hanbio (Hanbio, Shanghai, China) Lipofectamine 3000 (Invitrogen, Carlsbad, USA) were used to cell transfections. The sequences of siRNAs were listed in Table S1.

RNA isolation, reverse transcription, and qRT-PCR

Total RNA was isolated from cells and tissues using RNAiso Plus (Takara, Dalian, China) following the manufacturer's instructions. The integrity and purity of the extracted total RNA were determined using NanoDrop One UV-Vis spectrophotometer (Thermo Fisher Scientific, Waltham, USA). RNA was immediately stored at -80 °C until use. Reverse transcription was carried out using the All-in-One™ First-Strand cDNA Synthesis Kit (Uelandy, Suzhou, China). Genomic DNA was removed at 42 °C for 2 min. Subsequently, RNA from cells and tissues was reverse-transcribed into cDNA at 37 °C for 15 min, followed by an inactivation step at 85 °C for 5 s. qRT-PCR was performed using the QuantStudio 5 Real-Time PCR System (Applied Biosystems, Foster City, USA) and the Hieff qPCR SYBR Green Master Mix kit (Yeasen, Shanghai, China). The qRT-PCR reactions were conducted with an initial denaturation at 95 °C for 5 min, followed by 40 cycles of 95 °C for 10 s and annealing at 60 °C for 30 s. Primer sequences used for qRT-PCR are listed in Table S2. The relative quantification of RNA was calculated using the $2^{\wedge-\Delta\Delta Ct}$ method, with GAPDH as the internal reference.

Western blot analysis

Total protein was obtained by lysis of cells and centrifugation of tissue samples using RIPA buffer containing protease and phosphatase inhibitors on ice and homogenized with a BCA Kit (Beyotime, China). Denaturation by heat. SDS-PAGE gels were assembled in appropriate percentages based on the expected protein size range. The gel was run at a constant voltage of 100 V until the protein was sufficiently separated. The separated proteins were transferred from the gel to the PVDF membrane (Millipore, Massachusetts, USA) using a wet transfer system. 5% skim milk powder in 1xTBST was blocked at room temperature. The membranes were incubated overnight at 4℃ with the following primary antibodies: AKT (ab179463) from Abcam (MA, USA), anti-phospho-AKT (Ser473) (4060), anti-PDK1 (3062) and anti-E-cadherin (3195) from Cell Signaling Technology (MA, USA), anti-Palladin (No. 10853-1-AP), and anti-GAPDH (No. 10494-1-AP) from Proteintech (Wuhan, China). Membranes were incubated for 1 h in blocking buffer with a secondary antibody attached to HRP. Enhanced chemiluminescence reagents (Millipore, MA, USA) were used to visualize the protein bands. Protein band signals were captured using a chemiluminescence imaging system.

CircRNA identification

Total RNA and gDNA was extracted from CRC cells. Forward and reverse primers based on the specific junction sequence of the circular RNA for circKDM1A are designed to amplify the sequences in both cDNA and gDNA. The presence and specificity of the amplification products are validated using qRT-PCR and nucleic acid electrophoresis.

RNA Stability Assay: Cells are treated with 100 ng/mL actinomycin D (Merck, Darmstadt, Germany), and total RNA is harvested and extracted at 0 h, 8 h, 16 h, and 24 h post-treatment. The changes in circRNA expression levels are quantified using qRT-PCR.

Fluorescence in situ hybridization (FISH)

12 mm diameter coverslips are placed at the bottom of a 24-well plate, and an appropriate number of cells (6×10^4 cells/well) are cultured overnight. The cells are allowed to reach 60–70% confluency before the experiment. At room temperature, the cells are fixed with 4% paraformaldehyde in PBS for 20 min. The specific Cy3-labeled circKDM1A probe (Table S1) (GenePharma, Shanghai, China) is hybridized using a FISH kit (RiboBio, Guangzhou, China) according to the manufacturer's instructions. Briefly, pre-hybridization is performed at 37 °C for 30 min, followed by hybridization with 2.5 μL of 20 μM circKDM1A probe at 37 °C overnight. The cells are then stained with DAPI. Image acquisition is carried out using a laser scanning confocal microscope (Zeiss, Jena, Germany).

Immunohistochemistry (IHC) and paraffin –SweAMI -FISH + double IF

Paraffin sections were baked for 2 h, after deparaffinization, microwave repair cooling, permeabilization, and sealing, METTL1 primary antibody (No. 14994-1-AP, proteintech) or phospho-AKT primary antibody (GB150002-100, servicebio) was drip-added at low temperature overnight, and the signal was amplified by a DAB system (PV-6000D, Zsgb-bio, China). Imaged under a microscope (Olympus, Tokyo, Japan). A semi-quantitative ISH scoring criterion was used to assess METTL1 expression. METTL1 and phospho-AKTwere scored using Quant Center (3DHISTECH, Budapest, Hungary).

For Paraffin-SWEAMI-FISH+double IF, Paraffin sections were processed as above until antigen retrieval. The above FISH experimental procedures were completed. The cells were blocked by dropping BSA for 30 min. Primary antibody against METTL1 was added and incubated overnight at 4℃. Cy5-labeled secondary antibodies were incubated for 50 min at room temperature. The sections were blocked again and the PDK1 primary antibody was added dropfold at 4℃ overnight. Tsa-488-labeled secondary antibodies were incubated for 50 min at room temperature. DAPI was used to stain nuclei, and anti-fluorescence quenching sealing agent was added dropped-on to seal tablets. The sections were observed, and images were collected under a Nikon orthostatic fluorescence microscope.

RNA pull-down assay

The BersinBio™ RNA pulldown Kit (Bes5102) was used for the experiments. Biotinylated circKDM1A probe, biotinylated miR147b-3p probe, and their corresponding control probes were designed and synthesized by Genepharm (Shanghai, China) (Table S1). The RNA probes were heated to 95 °C for 2 min and then immediately placed on ice for 2 min to prepare RNA secondary structures. 40 μL of streptavidin magnetic beads were washed with NT2 buffer and then incubated with the RNA probes at 25 °C for 30 min. Cells were lysed in NT2 buffer containing protease inhibitors and RNase inhibitors, incubated on ice for 10 min, and then centrifuged. The supernatant was collected and incubated with the probe-bead complexes at 25 °C with gentle rotation for 2 h. The magnetic beads were collected and washed four times by adding 1 mL of NT2 buffer each time. Proteins were eluted by adding proteinase K and incubating at 55 °C for 30 min with intermittent mixing. RNA was extracted using the RNA Clean & Concentrator™-25 kit (R1017, ZYMO Research, USA) for subsequent qRT-PCR analysis.

RNA immunoprecipitation (RIP) assay

A total of 50 μl protein A/G beads were incubated with 5 μg (METTL1, AGO2) of the experimental antibody, or an equal amount of IgG antibody (Millipore, MA, USA) mixed at room temperature for 30 min. Cells were fully lysed using 1X RIP lysis buffer, and total cell lysates were mixed with the complexes described above and rotated overnight at 4℃. The beads were collected, and the supernatant was removed to add 1 ml 1x RIP wash buffer, and the beads were washed 6 times in total. Digestion was performed using proteinase k for 30 min. After digestion, RNA was purified using the RNA Clean & Concentrator™ kit (ZYMO Research, USA) to remove the enzyme and buffer components. The RNA was reverse transcribed using Revert Aid First Strand cDNA Synthesis Kit (Thermo Fisher Scientific, Carlsbad, CA, USA). Interactions between METTL1, AGO2, and circKDM1A transcripts were assessed by qPCR and normalized to the input.

m7G-circRNA meRIP

Total RNA was extracted from 2×10^7 cells. The RNA (2 μg) was treated with RNase R (4 U) (Epicentre Biotechnologies, Madison, WI, USA) at 37℃ for 15 min to digest linear RNA. Protein A/G magnetic beads were

blocked with PBS containing 5% BSA to prevent nonspecific binding. The beads were then coupled with the m7G antibody (RN017M, MBL) by rotating at room temperature for 1 h. RNA fragments from the RNase R digestion were incubated with the bead-antibody complexes at 4℃ for 4 h with gentle rotation. The beads were washed six times with 1x RIP wash buffer to remove nonspecifically bound RNA. The RNA/antibody complexes were digested with Proteinase K at 55℃for 30 min to remove proteins and release the RNA. After digestion, RNA was purified using the RNA Clean & Concentrator™ kit (ZYMO Research, USA) to remove the enzyme and buffer components. The RNA was reverse transcribed using Revert Aid First Strand cDNA Synthesis Kit (Thermo Fisher Scientific, Carlsbad, CA, USA). The enrichment of m7G-modified RNA was assessed by qRT-PCR and normalized to the input RNA.

Transwell assay

For cell migration assays, 5×10^5 modified HCT116 and SW480 cells were seeded in transwell chambers with an 8 μm well membrane (Corning, NY, USA). After 36–72 h of culture, the lower layer cells were fixed, and the upper layer cells were removed by wiping. Migrating cells were stained with Giemsa (Solarbio, Beijing, China). Images of the cells were obtained using light microscopy in four fields. Similarly, for invasion assays, 5×10^5 modified HCT116 and SW480 cells were seeded in transwell chambers with an 8 μm pore membrane (Corning, NY, USA) coated with Matrigel (Corning, NY, USA). The invasive cells were stained and imaged. The number of migrating cells and invasive cells were counted.

Edu and CCK8 assay

Edu experiments were performed with the support of Cell-Light TM Edu Apollo In Vitro Kit (C10310-1) (RiboBio, Guangzhou, China). According to the instructions, 2×10^3 modified HCT116 or SW480 cells were seeded in 96-well plates, the cells were cultured for 48 h, Edu labeling was added. Then, apollo staining and DNA staining was performed, and images of different channels were collected by fluorescence microscope (Olympus Corporation, Tokyo, Japan) and synthesized. For the CCK8 assay, 2000 modified HCT116 or SW480 cells were seeded in 96-well plates. After the cells were cultured for 0, 12, 24, 48, 72 and 96 h, the cells were added to the Cell Counting Kit-8 (Dojindo Laboratories, Kumamoto, Japan) and incubated at 37 °C for 2 h. The OD450 value was measured using a microplate detector.

Colony formation and cell cycle and apoptosis

For the clone formation assay, 2×10^3 modified CRC cells were seeded in 12-well plates. After 4 weeks, the cells had grown in groups, they were fixed, Giemsa stained, and photographs were taken. The number of communities was counted using Image J (National Institutes of Health, Bethesda, MD, USA). The apoptosis of modified HCT116 or SW480 cells was detected by Annexin V/propidium iodide (PI) apoptosis detection kit (Beyotime, Shanghai, China). After the cells were collected, FITC/mCherry-Annexin V and PI double staining were added and detected by flow cytometry (ACEA NoVoCyte, USA). The cell cycle experiment was conducted using the Cell Cycle Detection Kit (C6031, Uelandy) as per the manufacturer's instructions. Collected cells were fixed overnight in pre-cooled 70% ethanol. Following fixation, the cells were washed with PBS and stained with RNaseA and PI at room temperature for 30 min. Flow cytometry analysis was performed using the ACEA NovoCyte system (USA). The acquired data were analyzed and fitted using FlowJo™ software.

Animal models

EGFP-sh-METTL1, luci-lv-METTL1, mcherry-lv-circKDM1A, and mcherry-mut-circKDM1A plasmids, along with their respective control plasmids (Genepharm, Shanghai, China), were co-transfected with pSPAX2 and pMD2G plasmids into 293T cells for virus packaging. The concentrated viruses were then used to transduce HCT116 cells using LipoFilter Reagent (Hanbio Biotechnology, Wuhan, China). Stable cell lines were established by selecting with puromycin (2 μg/mL) or neomycin G418 (700 μg/mL). All mouse procedures were approved by the Institutional Animal Care and Use Committee of Zhengzhou University. BALB/c nude mice (4 weeks of age) were obtained from Vital River Laboratories. After a one-week acclimation period, the mice were injected via the tail vein with stable HCT116 cells (2×10^6 in 100 μL PBS) from each experimental group. The mice were regularly monitored for body weight and activity levels. The experiment was terminated if the mice showed significantly reduced activity, a body weight loss exceeding 20%, or severe cachexia. At the experimental endpoint, fluorescence was directly detected using the IVIS Illumina system (Caliper Life Sciences, USA), or bioluminescence was measured following intraperitoneal injection of D-luciferin (150 mg/kg, Yeasen, China). Mice from both the treatment and control groups were euthanized by overdose inhalation anesthesia. Lung metastases were harvested, fixed in paraffin, and sectioned for HE staining, immunohistochemistry, and immunofluorescence staining.

Statistical analysis

All data were analyzed using Prism 10.0 (GraphPad, San Diego, CA, USA) and expressed as mean±SD. Chi-squared tests were performed using SPSS Statistics 21 (IBM, Chicago, IL, USA). Significant differences between

two independent groups were evaluated by Student's t-test. Correlations were analyzed using Pearson's correlation coefficient(r) and two-tailed *P*-values. Survival curves were assessed by log-rank (Mantel-Cox) tests. $p<0.05$ was considered significant. All experiments were performed at least three times.

Results

M7G modification is enriched in circRNAs in CRC cells

To study the m7G modification in RNA level, we firstly performed m7G-RIP assays and further high-throughput sequencing to identify circRNA, lncRNA and mRNA (Fig. 1A). Interestingly, the results showed that there were abundant m7G modifications in circRNA (Fig. 1B). There were 937 identified circRNAs with m7G modification, and 62.4% circRNAs derived from exons (Fig. 1C). There were 1 to 15 m7G peaks in circRNAs (Fig. 1D). Most identified circRNA originated from chromosomes 1 and 2 (Fig. 1E). It has been reported that m7G modification in mRNA is enriched in a GA-rich context [18, 19]. Interestingly, we found the top m7G motif in circRNA was a GG-rich or GT-rich motif (Fig. 1F). To verify

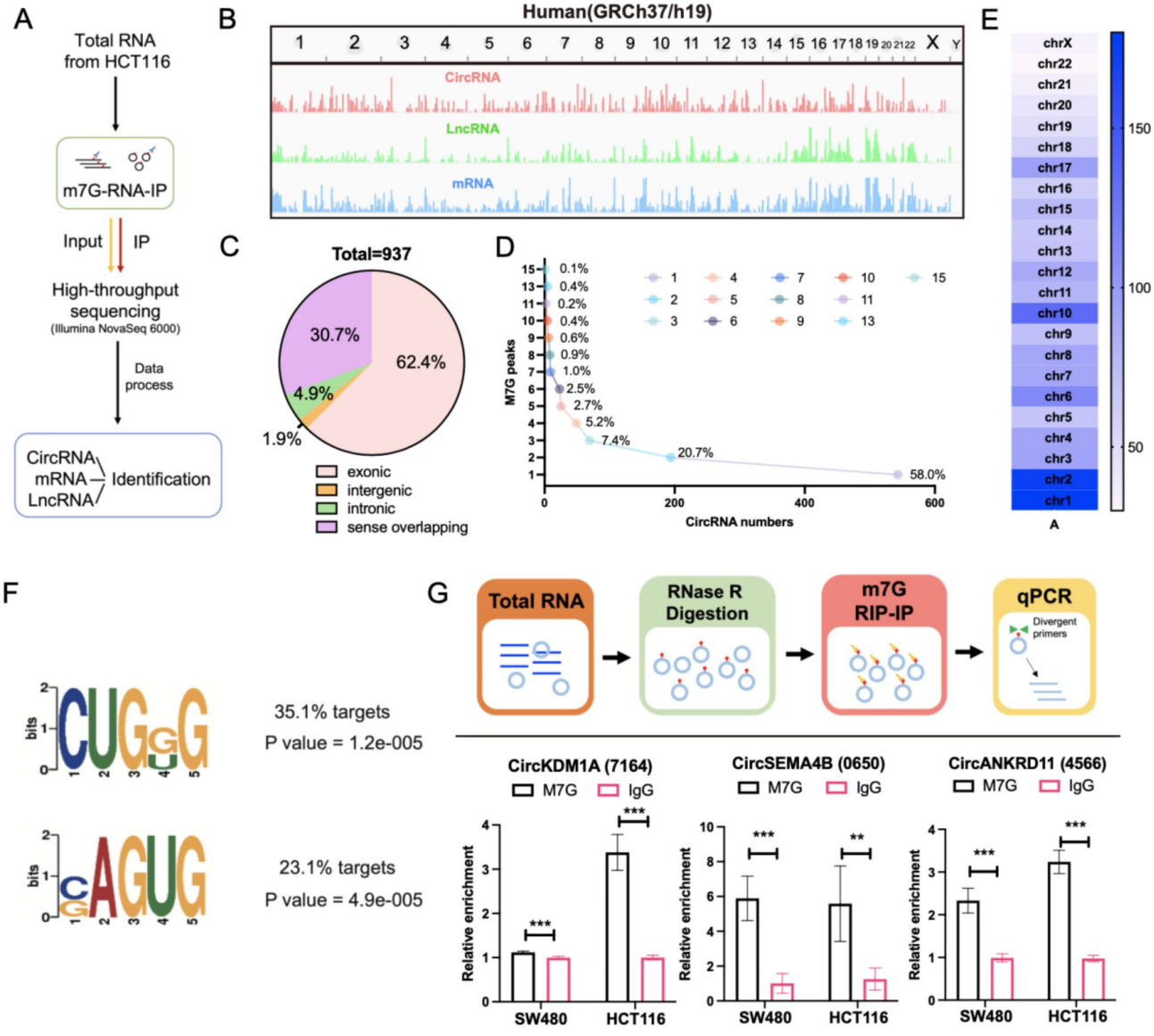

Fig. 1 Abundant m7G modification in circRNAs in CRC cells. **A**. The m7G-RNA immunoprecipitation library building protocol involves immunoprecipitating m7G-modified RNAs using an anti-m7G antibody. The enriched RNAs are then used to construct a sequencing library; **B**. Referencing the GRCh37/h19 version of the human genome, map the locations of m7G peaks and compare the distribution of m7G modifications across circRNA, lncRNA and mRNA; **C**. The proportion of m7G-modified circRNAs derived from different genomic regions, such as exons, introns, intergenic regions and sense overlap regions; **D**. Proportion of 15 types of m7G peaks on circRNA; **E**. The Distribution of circrnas containing m7G modification on each chromosome; **F**. The preference of m7G motifs on circRNAs for GG or GT sequences and their proportions; **G**. Validation of m7G modification on circKDM1A, circSEMA4B, and circANKRD11 in HCT116 and SW480 cells by m7G-RIP-qPCR. Mean ± SD. Student's t-test, $0.001 < **p < 0.01$, $***p < 0.001$

m7G modification in circRNA, we optimized the protocols of m7G-RIP (Fig. 1G). The m7G RIP-qPCR results showed that anti-m7G pulldowned the circKDM1A, circSEMA4B, and circANKRD11 in CRC cell lines (Fig. 1G). Taken together, these results illustrate that the m7G modification is enriched in circRNAs.

METTL1 as an oncogene in CRC to promote circRNA stability via m7G modification

Many studies proved that METTL1 as a methyltransferase deposit internal m7G modification in mRNAs and tRNA [19, 20]. METTL1 expression was upregulated in CRC through analyzing TCGA and GEO data (Fig. 2A and S1A). Our clinical cohort and previous whole transcriptome resequencing proved that METTL1 increased in CRC compared to peri-carcinomatous tissue (Fig. 2B and S1B). Moreover, higher-METTL1 patients were associated with poorer prognosis (Fig. 2C). Next, we explored METTL1 function in CRC cells using gene silence method (Figure S2A). The results showed that silencing METTL1 inhibited cancer cell proliferation (Figure S2B and S2C), and significantly suppressed the migration and invasion of cancer cells (Figure S2D). To further evaluate METTL1 effect in vivo, we successfully built stably transfected cell lines using overexpressed METTL1 lentivirus and silencing METTL1 lentivirus (Figure S2E). In line with the findings in vitro, silencing METTL1 in CRC cells decreased CRC lung metastasis in vivo (Fig. 2D-E and Figure S2F), and overexpressed METTL1 promoted CRC metastasis in mice (Fig. 2F-G and Figure S2G). Our results indicate METTL1 serves as an oncogene and is involved in CRC progression. To further confirm that the m7G modification of circRNA is catalyzed by METTL1, we constructed a METTL1 catalytically inactive plasmid based on reported study [21] (Fig. 2H). Then, the m7G-RIP results showed that m7G level in three circRNAs was increased in METTL1 wild group and decreased when the catalytic site of METTL1 was knocked down (Fig. 2I). Taken together, these results show that the m7G modification loaded in circRNAs is catalyzed by METTL1, which is an oncogene in CRC.

An METTL1-upregulated circRNA, circKDM1A, plays an oncogene role in CRC

Studies reported that the presence of m7G modification contributes to the stability of mRNA, tRNA and miRNA [18, 20, 21]. To clarify whether the presence of m7G modification affects the stability of circRNA, we knocked down the expression of METTL1 and performed RNA sequencing. The results showed that the global circRNA expression was downregulated by METTL1 siRNA (Figure S3A). Subsequently, we merged the data of m7G-RIP-seq and SiMETTL1-seq and found that 36 differentially expressed circRNAs had m7G modification (Fig. 3A and B). In order to further screen out circRNAs that potentially influence CRC progression, we used our previous sequencing data to identify the expression levels of the top seven differentially expressed circRNAs with the most abundant m7G. The results showed that circKDM1A was significantly more expressed in CRC tissues than that in adjacent areas (Fig. 3C and D). circKDM1A is derived from chromosome 1:23030469–23,050,520 and consists of 2 adjacent exons in the KDM1A gene (Figure S4A). To confirm the ring structure, we designed convergent and divergent primers and determined that circKDM1A exists as cDNA rather than gDNA (Figure S4B). Moreover, we further analyzed the expression of circKDM1A in 9 pairs of CRC tissues. ISH results showed that circKDM1A was highly expressed in CRC tissues (Fig. 3E and S4C). Higher expression of circKDM1A predicted poorer prognosis (Fig. 3F). To investigate the role of circKDM1A, we designed siRNA targeting the cross-linkage site of circRNA and performed in vitro functional experiments (Figure S4D). These results of clone, edu and flow cytometry experiments displayed that circKDM1A promoted CRC cell proliferation and inhibited cell apoptosis (Fig. 3G-J). Moreover, silencing circKDM1A impaired the ability of migration and invasion in CRC cells (Fig. 3K). Taken together, these data suggest that m7G modified circKDM1A plays an oncogene role in CRC.

CircKDM1A stability is regulated by METTL1 depended on GG motif

To explore the impact of m7G modification on circRNA stability, we constructed circKDM1A plasmid with GG mutation and GT mutation based on the above motif preference analysis results. Next, we performed the m7G-RIP assay and showed that the m7G modification level of circKDM1A decreased significantly after mutating GG of circKDM1A, while there was no change after mutating GT (Fig. 4A). Therefore, we speculate that GG is the m7G modification preference on circKDM1A. Then, we used RNAfold WebServer tool to analyze the stability of the secondary structure of circKDM1A. GG mutated circKDM1A exhibited higher minimum free energy (MFE) and thermodynamic ensemble (TE) than wild-type circKDM1A (Fig. 4B). Actinomycin D assay show that GG-mutated circKDM1A is less stable than wild-type circKDM1A (Fig. 4C). To confirm that the stability of circKDM1A is affected by m7G modification catalyzed by METTL1, we firstly examined the circKDM1A expression in si-METTL1 or overexpressing METTL1 cell. Knockdown of METTL1 significantly reduced the expression of circKDM1A, while overexpression of METTL1 showed the opposite trend (Fig. 4D). Meanwhile, circKDM1A was more stable in cells with overexpressing METTL1 than that in the control (Fig. 4E).

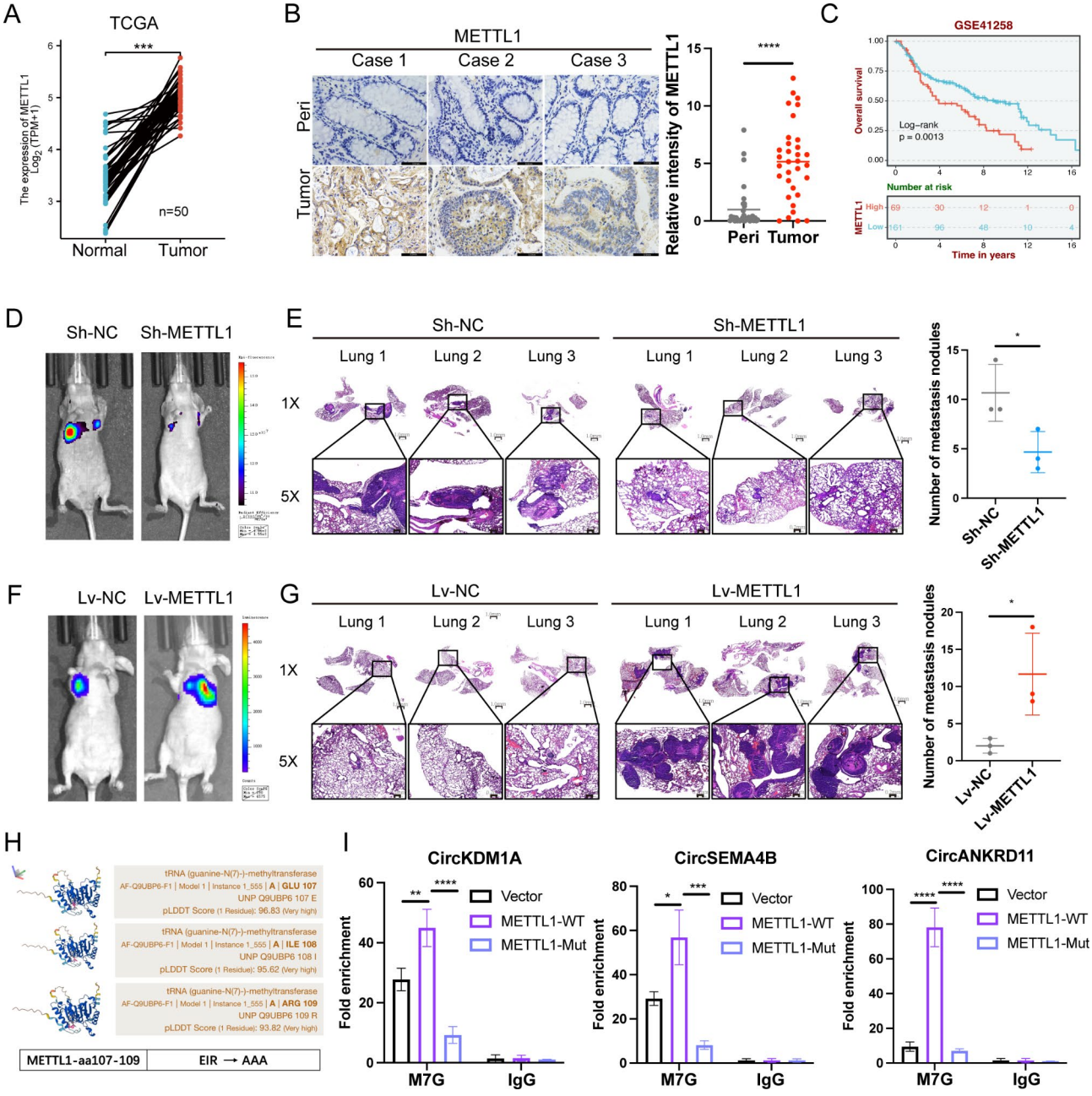

Fig. 2 Oncogenal METTL1 catalyzed m7G modification in circRNA to promote its expression. (**A**) The expression of METTL1 in CRC samples and corresponding control samples in the TCGA database ($n=50$); (**B**) Representative IHC images and the expression of METTL1 in CRC tissues compared to its paracancerous tissues ($n=33$); (**C**) The prognosis of METTL1 from GSE41258 in CRC; **D**. In vivo fluorescence imaging of BALB/c nude mice with stable GFP-METTL1-knocked down HCT116 cells or control cells via tail vein injection ($n=3$); **E**. HE staining and the number of metastatic nodules in the lungs of BALB/c nude mice ($n=3$); **F**. In vivo fluorescence imaging of BALB/c mice with stable luci-METTL1-overexpressing HCT116 cells or control cells via tail vein injection; **G**. HE staining and the number of metastatic nodules in the lungs of BALB/c nude mice ($n=3$); **H**. Schematic representation of the constructed mutant METTL1 plasmid, which mutated the M7G-modified domain of METTL1 catalytic from EIR to AAA; **I**. M7G-RIP and qRT-PCR were used to detect the effect of METTL1 active site mutation on the m7G modification of circKDM1A, circSEMA4B, and circANKRD11. Mean ± SD. Student's t-test, 0.001 < $^{**}p<0.01$, $^{***}p<0.001$

We next designed a rescue assay to detect m7G level after mutating the GG motif of circRNA in overexpressing METTL1 cells. Strikingly, Notably, we found that GG mutation on circRNA reduced the increase in m7G modification level caused by high METTL1 expression (Fig. 4F). We further performed rescue assay in the METTL1-overexpressed cells by silencing circKDM1A. Inhibiting circKDM1A rescues CRC cell proliferation, migration, and invasion in response to METTL1 overexpression (Fig. 4G and H, S4E and S4F). Taken together,

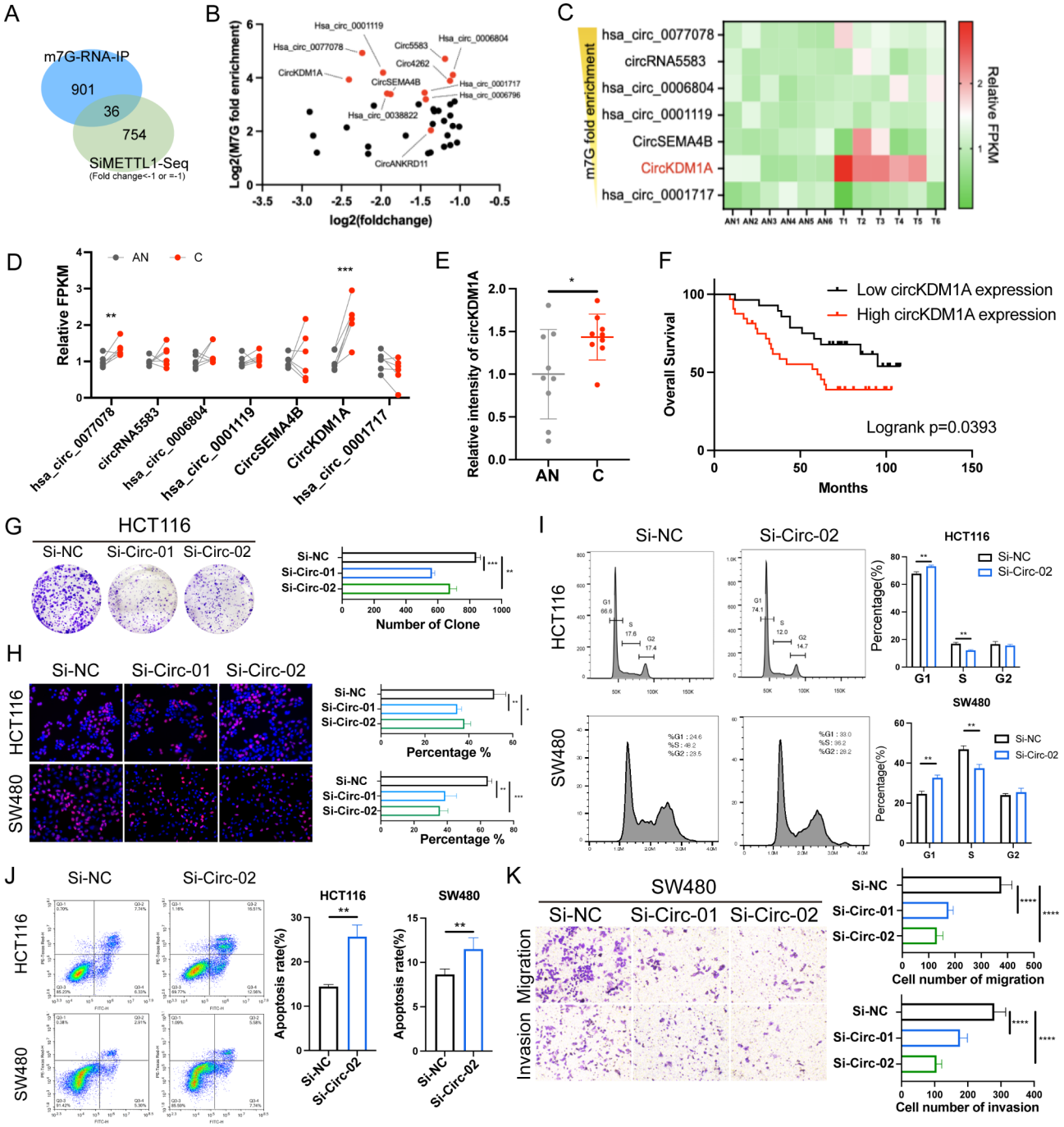

Fig. 3 Knocking down circKDM1A modified by m7G inhibited CRC progression. **A**. Venn diagram showing the intersection of RNAs significantly down-regulated RNAs from siMETTL1-seq and RNAs pulled down from m7G-RIP-seq; **B**. Enrichment degree of m7G on differently expressed circRNAs; **C**. Expression of 7 circRNAs with significantly enriched m7G in 6 pairs of CRC tissues Heat map; **D**. Differential expression of 7 m7G significantly enriched circRNAs in 6 pairs of CRC tissues. AN: adjacent area, C: cancer; **E**. Expression of circKDM1A in CRC tissues detected by qRT-PCR. AN: adjacent area, C: cancer; **F**. Prognosis of circKDM1A in a CRC clinical queue detected by a tissue microarray ($n = 60$); **G**. Effect of interfering with circKDM1A on CRC cells colony formation; **H**. Effect of interfering with circKDM1A on CRC cells proliferation detected by edu assay and the proportion of cells in the proliferation stage in each group; **I**. The effect of interfering with circKDM1A on CRC cells cycle using flow cytometry and the proportions of cells in G1 phase, S phase or G2 phase calculated by FlowJo™; **J**. The effect of interfering with circKDM1A on CRC cells apoptosis using flow cytometry and the proportions of cells in early and late apoptosis calculated by FlowJo™; **K**. Effects of interfering with circKDM1A on CRC cell invasion and migration detected by transwell assay. Mean ± SD. Student's t-test, $*p < 0.05$, $0.001 < **p < 0.01$, $***p < 0.001$, $****p < 0.0001$

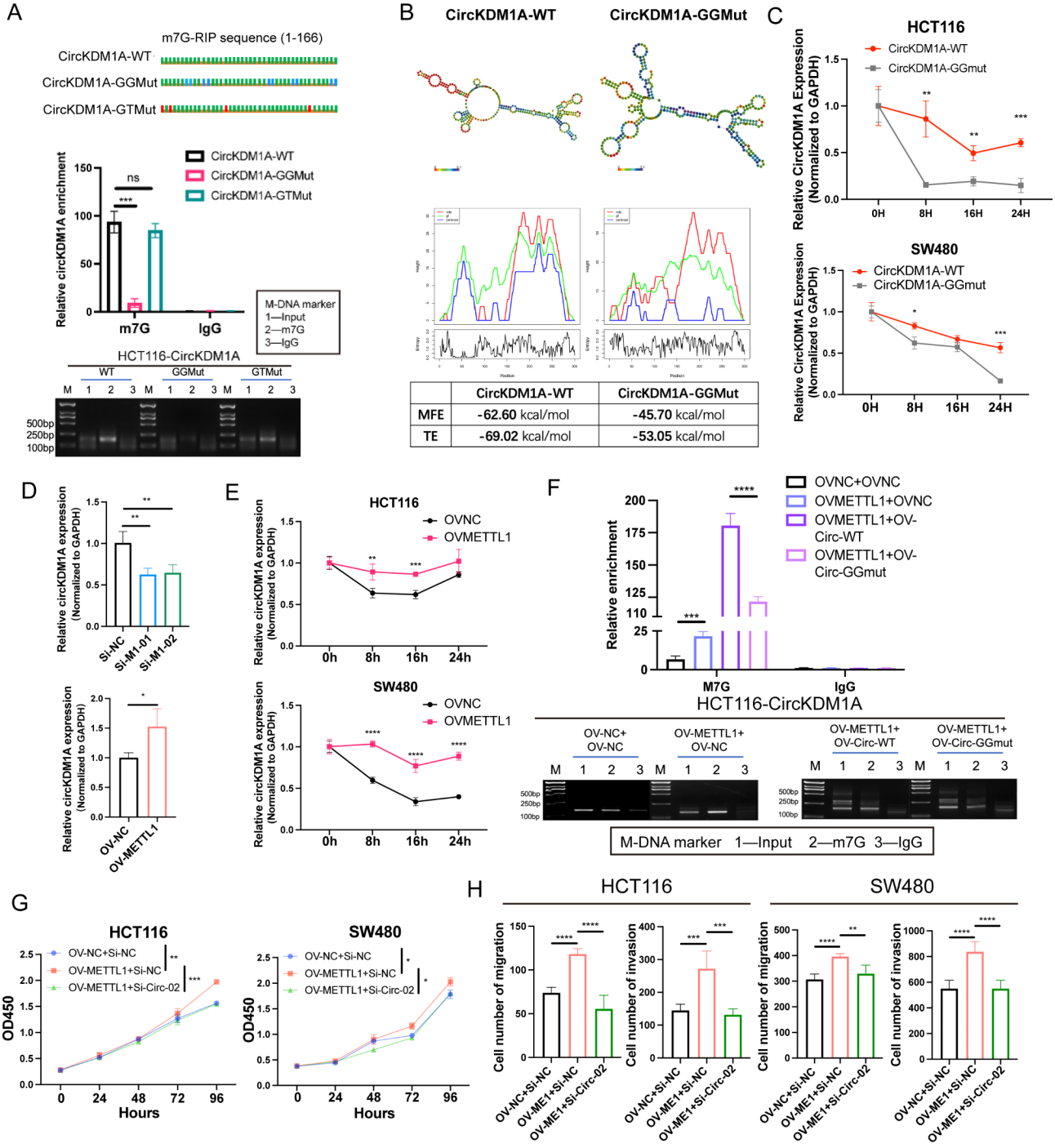

Fig. 4 The stability of circKDM1A is regulated by METTL1 through m7G modification. (**A**) Diagram for constructing mutant circKDM1A Plasmids with GG or GT Motifs and detection of mutant impact on m7G modification enrichment of circKDM1A using m7G-RIP and nucleic acid gel electrophoresis; (**B**) The RNA fold website simulates and predicts the stability of the secondary structure GG-mutated circKDM1A and wild-type; (**C**) Actinomycin D assay and qRT-PCR to analyze the stability of GG mutant circKDM1A and wild-type circKDM1A in CRC cells; (**D**) Effects of interference and overexpression of METTL1 on circKDM1A expression by qRT-PCR; (**E**) Actinomycin D experiment and qRT-PCR to analyze the effect of overexpression of METTL1 on the stability of circKDM1A in CRC cells; (**F**) The impact of the m7G active site mutation of METTL1 and the GG mutation of circKDM1A on the M7G modification of circKDM1A by M7G-RIP and nucleic acid gel electrophoresis; (**G**) Effects on cell proliferation after knocking down circKDM1A in cells with high expression of METTL1 detected by CCK8; **H**. Effects of knocking down circKDM1A in cells with high expression of METTL1 on cell invasion and migration detected by transwell assay. Mean ± SD. Student's t-test, $*p < 0.05$, $0.001 < **p < 0.01$, $***p < 0.001$, $****p < 0.0001$, no significance (ns)

our results illustrate that METTL1 promotes the stability of circKDM1A through GG-dependent m7G modification. Moreover, circKDM1A is a key collaborator for METTL1 to promote CRC progression.

M7G-modified circKDM1A activated AKT pathway by upregulated PDK1

To explore the molecular mechanism that circKDM1A promotes CRC progresssion, we firstly analyzed the distribution of circKDM1A in CRC cells. Cell localization experiments showed that circKDM1A was mainly distributed in the cytoplasm, and a small amount also exists in the nucleus (Fig. 5A and B). Previously reported that cytoplasmic circRNA can act as a sponge to adsorb miRNA, bind to protein, or translate small peptides. We next explored whether circKDM1A in the cytoplasm could sponge miRNA. Therefore, we performed RIP experiments and found that circKDM1A bound AGO2 protein, which suggested that circKDM1A has the potential to serve as a sponge (Fig. 5C). Then, we used the Circinteractome (https://circinteractome.nia.nih.gov/) to predict the miRNAs that circKDM1A may bind to. According to the context+score, we found that the top three miRNAs potentially binding to circKDM1A were miR-147b-3p, miR-625-5p and miR-526b-5p (Fig. 5D). We then designed a circRNA biotin probe across the circKDM1A junction site and used circRNA pull down assay to determine the targeted miRNA (Figure S5A). The CircKDM1A probe enriched more miR-147b-3p than the NC probe (Fig. 5E). Additionally, silencing METTL1 or overexpressing METTL1 in CRC cells leads to differential expression of miR-147b-3p (Figure S5B). In order to explore the molecular mechanism of m7G-modified circKDM1A, we performed KEGG pathway enrichment based on the sequencing data of siMETTL1. Among the top 20 signaling pathways, PI3K-Akt signaling pathway was enriched and was regulated by METTL1 and circKDM1A (Figure S5C, S5D and 5F). Then, we focused on PDK1, a potential target of miR-147b-3p in Targetscan database, and the upstream activator of Akt. Similarly, silencing circKDM1A or METTL1, as well as overexpressing circKDM1A or METTL1 in CRC cells, results in differential expression of PDK1 (Fig. 5G and S5E). Moreover, miR-147b-3p probe pulled down circKDM1A and PDK1 (Figure S5F and 5H). Upregulated PDK1 in overexpressing circKDM1A cells was inhibited by miR-147b-3p mimic (Figure S5G). Furthermore, the miR-147b-3p inhibitor can rescue the downregulation of PDK1 in circKDM1A knockdown cells (Figure S5H). To determine whether circKDM1A affected tumor suppressor-related proteins by upregulating PDK1, we designed siRNA of PDK1 to perform rescue experiments. In highly expressed circKDM1A cells, the activated AKT pathway was inhibited by siPDK1, and the expression of tumor suppressor proteins was increased (Figure S5I and Fig. 5I). Moreover, MK2206, the Akt inhibitor, could rescue the change of tumor suppressor-related proteins and cell mobility caused by overexpressed circKDM1A in CRC cells (Fig. 5J and S5J). Taken together, these data proved that m7G-rich circKDM1A played an oncogene role by upregulating PDK1 to activate AKT pathway in CRC cells.

Mutating m7G site in circKDM1A reduces its cancer-promoting ability

In order to explore the impact of m7G modification on the cancer-promoting ability of circRNA, we analyzed the CRC function change of circKDM1A mutated in the m7G modification site in vivo and in vitro. Our results displayed that GG mutated circKDM1A inhibited CRC cell proliferation and promoted cell apoptosis (Fig. 6A and B). Compared with the wild-type group, tumor cells in the mutant circKDM1A group showed worse invasion and migration abilities (Fig. 6C and D). Additionally, tumor cells in the mutant circKDM1A group exhibit significantly upregulated miR-147b-3p expression, while PDK1 expression is downregulated (Figures S6A and S6B). Then, we constructed wild-type and GG mutant circKDM1A stably transfected cell lines to explore the impact of GG mutant circKDM1A on CRC progression in vivo (Fig. 6E). We found less lung nodules in GG mutant circKDM1A group (Fig. 6F and G). Moreover, we found that METTL1 and circKDM1A have the same region in mouse lung nodules, and the highly expressed circKDM1A showed high expression of PDK1 (Fig. 6H and Figures S6K-M). Meanwhile, when GG motif in circKDM1A was mutated, METTL1 and circKDM1A were not found to have the same region and PDK1 expression was low (Fig. 6H and Figures S6K-M). In clinical specimens of CRC, the expression the correlation of METTL1-circKDM1A-miR-147b-3p-PDK1-p-AKT was further confirmed. The results indicated positive correlations between circKDM1A and METTL1, PDK1, and p-AKT, and a negative correlation with miR147b-3p (Fig. S6C-F). Similarly, METTL1 exhibited positive correlations with PDK1 and p-AKT and a negative correlation with miR147b-3p (Fig. S6G-I). MiR147b-3p demonstrated a negative correlation with PDK1 (Fig. S6J). Taken together, m7G modification is a key factor for circKDM1A to promote CRC progression.

Discussion

Here, we found that m7G modification is abundantly enriched in circRNAs. Remarkably, METTTL1, an oncogene in CRC, is responsible for catalyzing m7G modification on circRNAs. Then, we screened out a highly expressed circRNA in CRC, circKDM1A. We found that METTL1 lead to high expression of circKDM1A

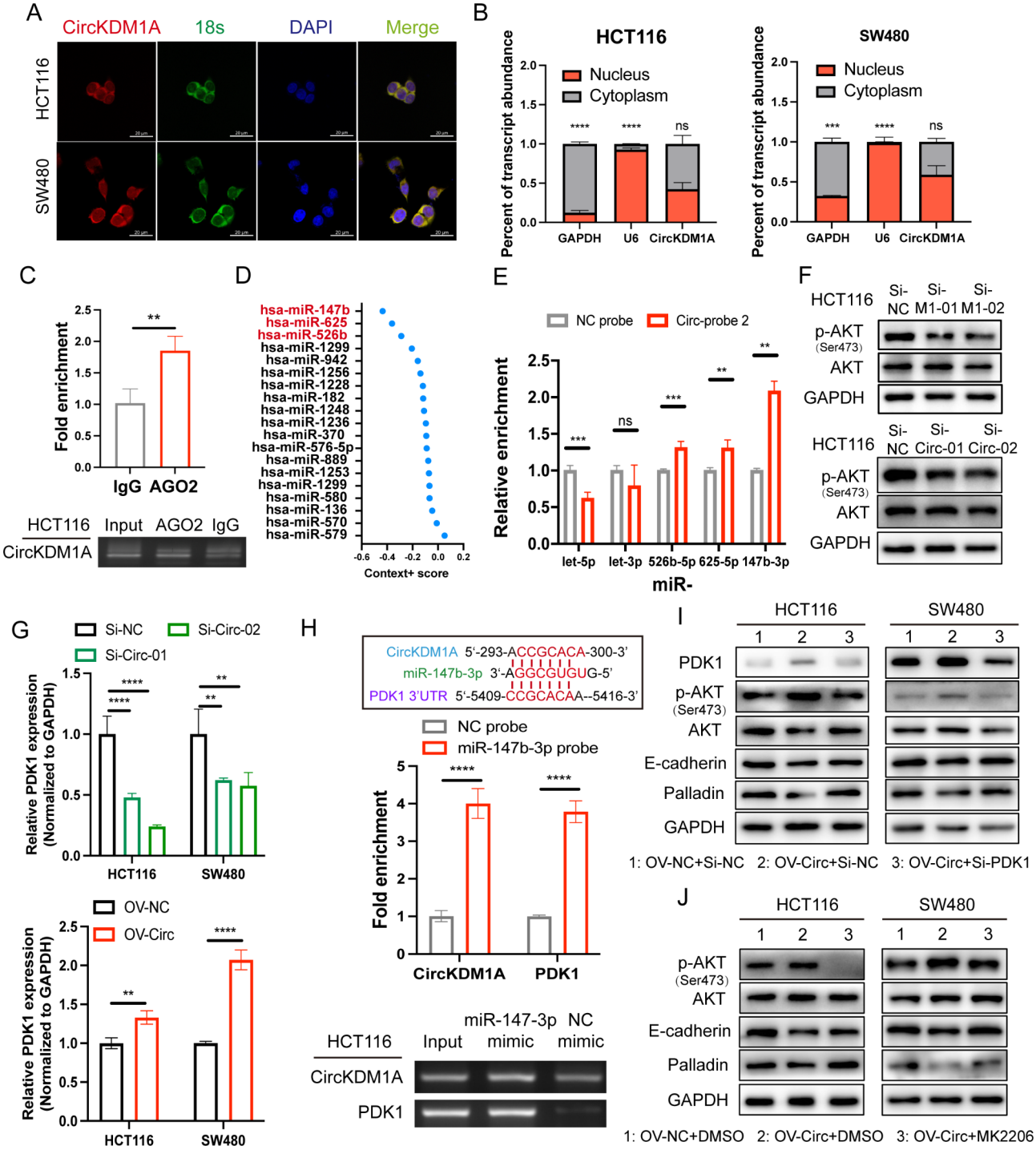

Fig. 5 CircKDM1A activated AKT pathway by upregulated PDK1. (**A**) The distribution of circKDM1A was demonstrated in the nucleus and cytoplasm of CRC cells used by Fluorescence in situ hybridization; (**B**) Nuclear-cytoplasmic separation experiment detects the distribution of circKDM1A in CRC cells; (**C**) The AGO2-RIP experiment was conducted to detect the enrichment fold of circKDM1A, followed by verification using nucleic acid gel electrophoresis; (**D**) Use the circinteractome website to predict the circKDM1A-targeted miRNAs; (**E**) CircRNA pulldown experiments confirm the interaction between circKDM1A and miR-526b-3p, miR-625-5p, and miR-147b-3p, with has-let-5p and has-let-3p serving as negative controls; (**F**) Effects of interfering with METTL1 and circRNA on the AKT pathway detected by Western Blot; (**G**) Effects of interference and overexpression of circKDM1A on PDK1 detected by qRT-PCR; (**H**) Pulldown experiment of miR-147b-3p to verify the binding of miR-147b-3p to circKDM1A and PDK1, followed by verification using nucleic acid gel electrophoresis; (**I**) Effects of knocking down PDK1 in cells with high expression of circKDM1A on PDK1, p-AKT and tumor suppressor proteins detected by Western Blot; (**J**) Effects of adding a AKT activity inhibitor (MK2206) to pAKT and tumor suppressor proteins in cells with high expression of circKDM1A detected by Western Blot; Mean ± SD. Student's t-test, $*p < 0.05$, $0.001 < **p < 0.01$, $***p < 0.001$, $****p < 0.0001$

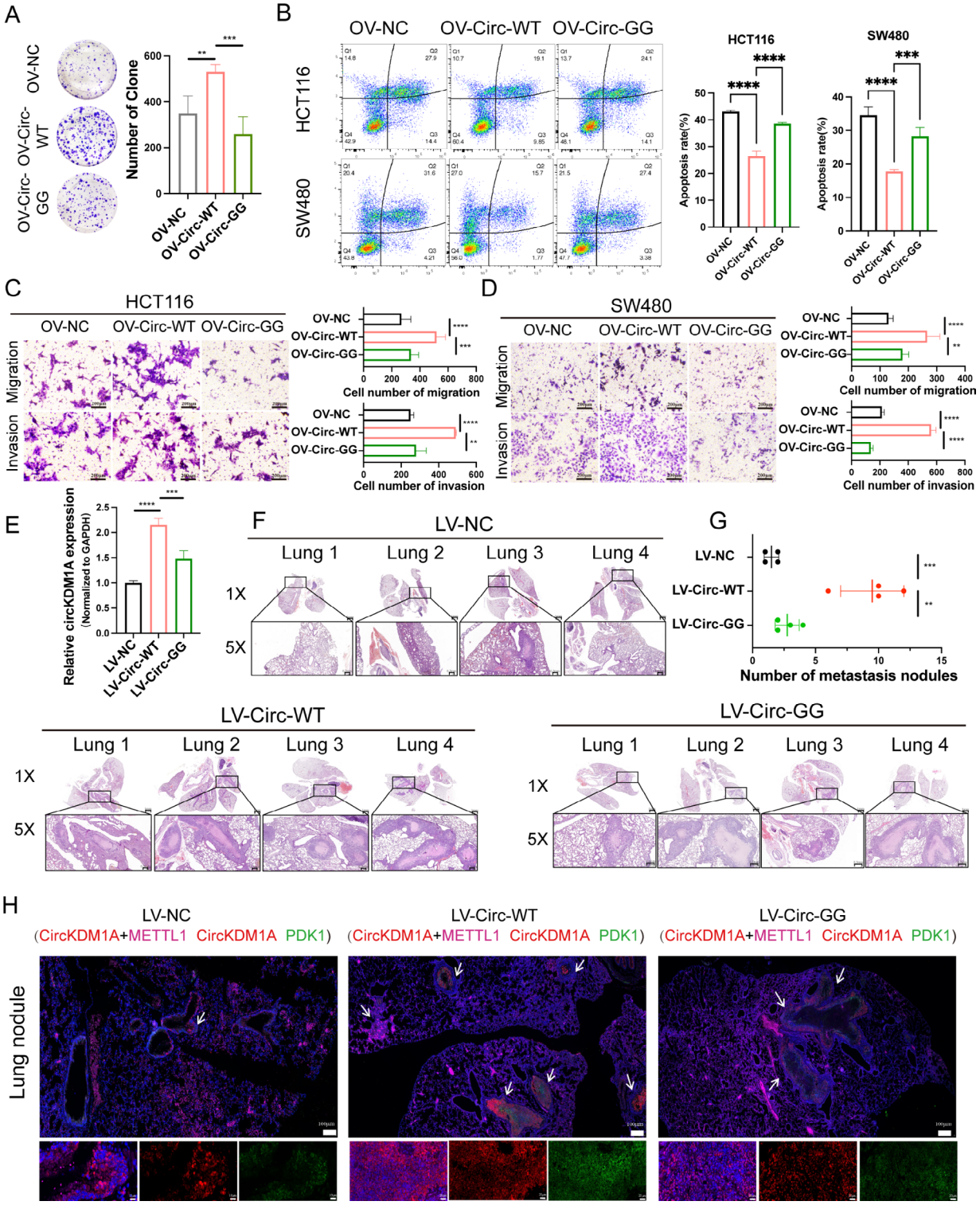

Fig. 6 m7G modified circKDM1A enhanced CRC progression. (**A**) Effect of GG mutation of circKDM1A on CRC cells clonality and the number of clone groups formed by CRC cells; (**B**) The effect of the GG mutation in the circKDM1A gene on apoptosis in CRC cells using flow cytometry and the proportions of cells in early and late apoptosis calculated by FlowJo™; **C**, **D**. Effect of GG mutation of circKDM1A on CRC cells invasion and migration detected by transwell assays and the number of migration and invasion was counted in CRC cells; **E**. The expression level of circKDM1A in the stable cell lines lv-nc, lv-circ-WT, and lv-circ-GG was detected using qRT-PCR; **F**. The effect of GG mutation of circKDM1A gene on lung metastasis in vivo was observed by panoramic scanning of HE staining and local magnification ($n=4$); **G**. The numbers of lung metastatic nodules in each group of mice ($n=4$); **H**. FISH-Multicolor immunohistochemistry analysis of the relationship among METTL1, circKDM1A, and PDK1 in pulmonary metastatic nodules in mice ($n=4$). Mean ± SD. Student's t-test, $0.001 < **p < 0.01$, $***p < 0.001$, $****p < 0.0001$

by promoting its stability in CRC. Interestingly, the stability of circKDM1A is regulated by the GG motif on circKDM1A. When circKDM1A is interfered with, the cancer-promoting effect of circKDM1A is weakened. Subsequently, we confirmed that circKDM1A upregulated the expression of PDK1 by adsorbing miR-147b-3p,

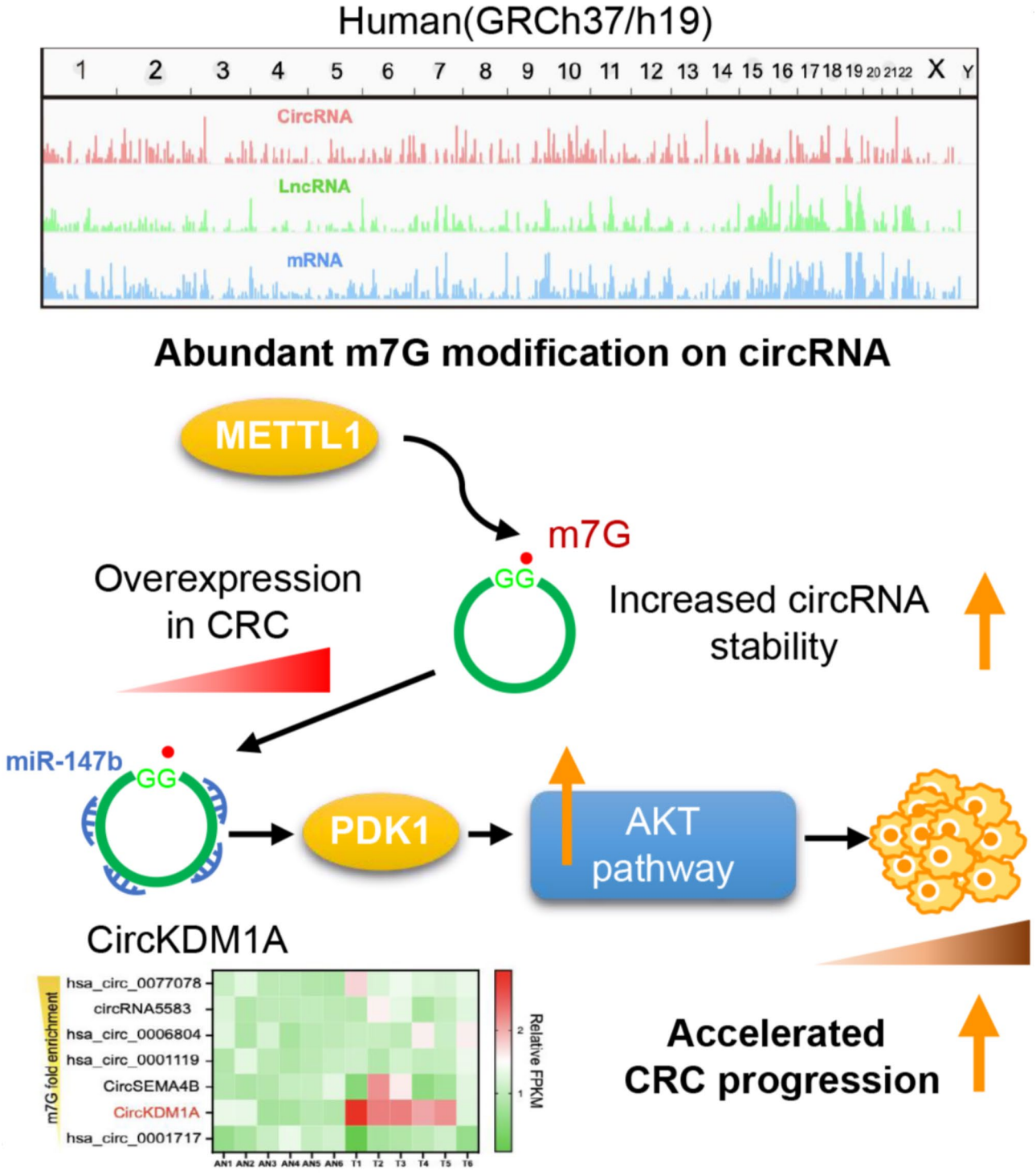

Fig. 7 Pattern diagram of the proposed mechanism in this study

thereby activating the AKT pathway. We further verified that the cancer-promoting effect of circKDM1A depends on the AKT pathway. Moreover, we found that m7G modification is a key factor for circKDM1A to promote cancer progression. Studies reported that METTL1 promotes tumor progression in various ways. Here, our study highlights that METTL1 participates in CRC progression by regulating the circRNA metabolism (Fig. 7).

RNA is one of the important molecules in living organisms. It is responsible for converting the genetic information in DNA into proteins. The production and degradation processes of RNA are tightly regulated, and the degradation process is critical for maintaining gene homeostasis and clearing defective RNAs. In the process of RNA metabolism, RNA modification play an important role and participate in the splicing, modification, storage, and degradation of RNA metabolism [2, 22]. CircRNA, which plays an important role in tumor progression, has been found to be regulated by m6A modification [23, 24]. In our early studies, we found that m6A modification can promote the formation of circRNA to accelerate CRC progression [8]. In addition, other groups have reported that the presence of m6A modification promotes the cytoplasmic export of circRNA [12]. However, whether the metabolism of circRNA is subject to other modifications has not been reported. M7G modification which is one of the most prevalent RNA modifications has received significant attention recently. In this study, we firstly reported that m7G is enriched in circRNAs, and the optimized m7GRIP confirmed this view.

Among the regulatory molecules involved in m7G modification, METTL1 is the most reported molecule and plays a cancer-promoting role in a variety of tumors [22]. However, the role of METTL1 in CRC remains unclear. In this study, we found that METTL1 is highly expressed in CRC and promotes CRC tumor progression. Moreover, we identified that METTL1 is responsible for catalyzing the m7G modification on circRNAs. The existence of this modification promotes the stability of a cancer-promoting circRNA, circKDM1A. Numerous studies have proven that circRNA plays an important regulatory role in the process of CRC by regulating downstream genes and cell signaling pathways [25–27]. circRNA mainly participates in tumor progression by adsorbing miRNA, binding to proteins, and translating into small peptides. In our study, we found that circKDM1A located in the cytoplasm can bind to AGO2 and adsorb miR-147b-3p to activate the AKT pathway to promote the progression of CRC. More interestingly, we found that m7G RNA modification is an essential factor in circKDM1A promoting CRC progression.

Conclusion

In this study, we found that circRNA is enriched in m7G modification, which was catalyzed by the m7G regulatory molecule METTL1. We report for the first time that METTL1 plays a cancer-promoting role in CRC. Moreover, METTL1 promotes the stability of a new cancer-promoting circRNA, circKDM1A, through regulating m7G modification. Subsequently, circKDM1A promoted CRC progression by activating the AKT pathway by adsorbing miR-147b-3p. More interestingly, the cancer-promoting effect of circKDM1A is regulated by m7G modification. Overall, this study discovered an important theory that METTL1 participates in circRNA metabolism to promote CRC progression, which provide a potential therapeutic target for CRC. In our work, we found more interesting finding and will explore the important role of m7G modification in circRNA encoding small peptides.

Supplementary Information

The online version contains supplementary material available at https://doi.org/10.1186/s12943-024-02090-z.

Supplementary Material 1

Supplementary Material 2

Supplementary Material 3

Supplementary Material 4

Supplementary Material 5

Author contributions

ZQS, YXX, and CHS contributed equally to this work. Conceptualization: ZQS, CZW, and CC; Investigation and Data Analysis: ZQS, YXX and CHS; Bioinformatics tool: XKW; Visualization: YXG; Original Writing: YXX and CC; Funding Acquisition: ZQS. All authors reviewed the manuscript.

Funding

This study was supported by The Provincial and Ministry Co-constructed Key Projects of Henan Medical Science and Technology (SBGJ202102134, SBGJ202102121), Henan Province Young and Middle-aged Health Science and Technology Innovation Leading Talent Project (YXKC2022016, YXKC2022004), The National Natural Science Foundation of China (81972663, 82173055), Scientific Research and Innovation Team of The First Affiliated Hospital of Zhengzhou University (ZYCXTD2023017), The Youth Talent Innovation Team Support Program of Zhengzhou University (32320290), Henan Medical Technology Popularization Project (SYJS2022109), Henan Provincial Health and Health Commission Joint Construction Project (LHGJ20200158), and Henan Province Health Young and Middle-Aged Discipline Leader Project (HNSWJW-2022018).

Data availability

No datasets were generated or analysed during the current study.

Declarations

Ethics approval and consent to participate

This study was approved by the Ethics Committee of the First Affiliated Hospital of Zhengzhou University (2019-KY-423), and all patients obtained informed consent before enrollment. All mouse procedures were approved by the Institutional Animal Care and Use Committee of Zhengzhou University.

Consent for publication

All patients obtained informed consent before enrollment.

Competing interests
The authors declare no competing interests.

Received: 12 May 2024 / Accepted: 14 August 2024
Published online: 30 August 2024

References

1. Siegel RL, et al. Cancer statistics, 2023. Cancer J Clin. 2023;73(1):17–48.
2. Roundtree IA, et al. Dynamic RNA modifications in gene expression regulation. Cell. 2017;169(7):1187–200.
3. Du H, et al. YTHDF2 destabilizes m(6)A-containing RNA through direct recruitment of the CCR4-NOT deadenylase complex. Nat Commun. 2016;7:12626.
4. Park OH et al. Endoribonucleolytic cleavage of m6A-Containing RNAs by RNase P/MRP complex. Mol Cell. 2019;74(3).
5. Mauer J, et al. Reversible methylation of m6Am in the 5′ cap controls mRNA stability. Nature. 2017;541(7637):371–5.
6. Li J, et al. Structural basis of regulated m7G tRNA modification by METTL1-WDR4. Nature. 2023;613(7943):391–7.
7. Li Z, et al. CircMETTL3, upregulated in a m6A-dependent manner, promotes breast cancer progression. Int J Biol Sci. 2021;17(5):1178–90.
8. Chen C, et al. N6-methyladenosine-induced circ1662 promotes metastasis of colorectal cancer by accelerating YAP1 nuclear localization. Theranostics. 2021;11(9):4298–315.
9. Liu H, et al. Circular RNA circDLC1 inhibits MMP1-mediated liver cancer progression via interaction with HuR. Theranostics. 2021;11(3):1396–411.
10. Wu P, et al. N6-methyladenosine modification of circCUX1 confers radioresistance of hypopharyngeal squamous cell carcinoma through caspase1 pathway. Cell Death Dis. 2021;12(4):298.
11. Xu J, et al. N(6)-methyladenosine-modified CircRNA-SORE sustains sorafenib resistance in hepatocellular carcinoma by regulating β-catenin signaling. Mol Cancer. 2020;19(1):163.
12. Chen RX, et al. N(6)-methyladenosine modification of circNSUN2 facilitates cytoplasmic export and stabilizes HMGA2 to promote colorectal liver metastasis. Nat Commun. 2019;10(1):4695.
13. Orellana EA, et al. METTL1-mediated m(7)G modification of Arg-TCT tRNA drives oncogenic transformation. Mol Cell. 2021;81(16):3323–e333814.
14. Chen B, et al. N(7)-methylguanosine tRNA modification promotes tumorigenesis and chemoresistance through WNT/β-catenin pathway in nasopharyngeal carcinoma. Oncogene. 2022;41(15):2239–53.
15. Ying X, et al. METTL1-m(7) G-EGFR/EFEMP1 axis promotes the bladder cancer development. Clin Transl Med. 2021;11(12):e675.
16. Chen Z, et al. METTL1 promotes hepatocarcinogenesis via m(7) G tRNA modification-dependent translation control. Clin Transl Med. 2021;11(12):e661.
17. Ma J, et al. METTL1/WDR4-mediated m(7)G tRNA modifications and m(7)G codon usage promote mRNA translation and lung cancer progression. Mol Ther. 2021;29(12):3422–35.
18. Malbec L, et al. Dynamic methylome of internal mRNA N7-methylguanosine and its regulatory role in translation. Cell Res. 2019;29(11):927–41.
19. Zhang L-S et al. Transcriptome-wide mapping of internal N7-methylguanosine methylome in mammalian mRNA. Mol Cell. 2019;74(6).
20. Orellana EA et al. METTL1-mediated m7G modification of Arg-TCT tRNA drives oncogenic transformation. Mol Cell. 2021;81(16).
21. Pandolfini L et al. METTL1 promotes let-7 MicroRNA Processing via m7G methylation. Mol Cell, 2019. 74(6).
22. Luo Y, et al. The potential role of N7-methylguanosine (m7G) in cancer. J Hematol Oncol. 2022;15(1):63.
23. Chen Y, et al. Activation of YAP1 by N6-methyladenosine-modified circCPSF6 drives malignancy in hepatocellular carcinoma. Cancer Res. 2022;82(4):599–614.
24. Chen X, et al. m6A modification of circSPECC1 suppresses RPE oxidative damage and maintains retinal homeostasis. Cell Rep. 2022;41(7):111671.
25. Long F, et al. Comprehensive landscape and future perspectives of circular RNAs in colorectal cancer. Mol Cancer. 2021;20(1):26.
26. Kristensen LS, et al. The emerging roles of circRNAs in cancer and oncology. Nat Rev Clin Oncol. 2022;19(3):188–206.
27. Liu Z, Weng, S et al. BEST: a web application for comprehensive biomarker exploration on large-scale data in solid tumors. J Big Data. 2023;10:165.

Publisher's note